OPEN ACCESS
Journal of Multidisciplinary Applied Natural Science Vol. 6 No. 2 (2026) https://doi.org/10.47352/jmans.2774-3047.373
Check for updates
Research Article

Probabilistic Modeling of Annual Maximum Rainfall for Intensity-Duration-Frequency Curve Construction in the Mamminasata Region, South Sulawesi Province, Indonesia

Wahidah Sanusi*, Sudarmin Patahuddin, and Sahlan Sidjara

Received : September 28, 2025	Revised : December 24, 2025	Accepted : February 9, 2026	Online : March 19, 2026

Abstract
The evaluation of extreme rainfall events is crucial for the management and planning of water resources, particularly in the design of drainage systems and water storage reservoirs. Such evaluation can be carried out through the estimation of design rainfall, which is commonly represented as rainfall intensity–duration–frequency (IDF) data. The purpose of this study is not only to apply probabilistic models to annual maximum daily rainfall data but also to construct the IDF curves of rainfall in the Mamminasata region of South Sulawesi Province. This study utilizes annual maximum daily rainfall data obtained from the Water Resources, Human Settlements, Spatial Planning, and Development Office of South Sulawesi Province, as well as the Meteorology, Climatology, and Geophysics Agency (BMKG) of Indonesia. The dataset consists of observations from 8 rainfall stations in the Mamminasata region spanning 36 years, from 1989 to 2024. The methodology involves first determining the appropriate probability distribution for each rainfall station, followed by estimating rainfall intensity using the Mononobe method, and finally constructing the IDF curves based on the estimated design rainfall and rainfall intensities for different return periods. This study found that each regency or city within the Mamminasata region generally exhibits distinct rainfall probability distributions. This highlights the importance of evaluating multiple probabilistic models to appropriately characterize the variability and extremes rainfall pattern across different locations. Based on the IDF curve, the results indicate that the longer the rainfall duration, the lower the intensity. Likewise, the shorter the return period, the lower the corresponding intensity.

Keywords: IDF curve, maximum rainfall, Mononobe method, probabilistic model

1. INTRODUCTION

Extreme rainfall events can lead to both droughts and floods. These events recur almost every year, as observed in the Mamminasata region of South Sulawesi, where heavy rainfall with high intensity struck the city of Makassar in mid-December 2024 and early 2025, resulting in flooding across 11 districts. The flood that hit Makassar at that time was the most severe compared to previous years. It also caused several areas to become paralyzed and inaccessible, with hundreds of vehicles stranded in Maros Regency. In Gowa Regency, residents living near the Bilibili River were evacuated to safe locations [1]-[3]. Meanwhile, heavy rain accompanied by strong winds also affected Takalar Regency, causing flooding in several areas with water levels reaching approximately 70 cm [4].

One approach that can be used to understand extreme rainfall patterns is the intensity–duration–frequency (IDF) curve analysis [5]. The IDF curve is a statistical tool that estimates the magnitude of extreme rainfall that may occur over different durations and intensities, and it provides information on rainfall intensity for various return periods [5]-[7]. Information derived from the IDF curve is particularly useful in the design of drainage infrastructure and flood control systems [7]. Proper management and planning are expected to minimize flooding or waterlogging in an area, while excess water can also be directed to infiltration or storage, so that it may be utilized during the dry season.

Many hydrological researchers have conducted studies on the IDF relationship of rainfall. For example, Al Mamoon et al. [8] estimated new design rainfall in Qatar using L-moments based on the frequency index approach, while Elsebaie [9] developed IDF relationships for 2 regions in Saudi Arabia. Similarly, De Paola et al. [10] evaluated IDF curves for 3 regions in an African city. As previously explained, the IDF relationship encompasses rainfall intensity, varying durations, and the recurrence intervals of extreme rainfall

Publisher's Note:
Pandawa Institute stays neutral with regard to jurisdictional claims in published maps and institutional affiliations.

Copyright:
© 2026 by the author(s).
Licensee Pandawa Institute, Metro, Indonesia. This article is an open access article distributed under the terms and conditions of the Creative Commons Attribution (CC BY) license (https://creativecommons.org/licenses/by/4.0/).

Table 1. Name and location of study.

Code	Name of station	Regency/City	Longitude	Latitude	Elevation (m a.s.l.)
St. 1	Camba	Maros	119.839	-4.921	338
St. 2	Panyalingan	Maros	119.563	-4.918	1
St. 3	Maroangin	Maros	119.583	-4.967	3
St. 4	Paotere	Makassar	119.420	-5.114	4
St. 5	Bontosallang	Gowa	119.414	-5.331	16
St. 6	Paku	Gowa	119.450	-5.283	18
St. 7	Sungguminasa	Gowa	119.461	-5.209	13
St. 8	Palleko	Takalar	119.463	-5.358	16
St. 9	Campagaya	Takalar	119.395	-5.346	12

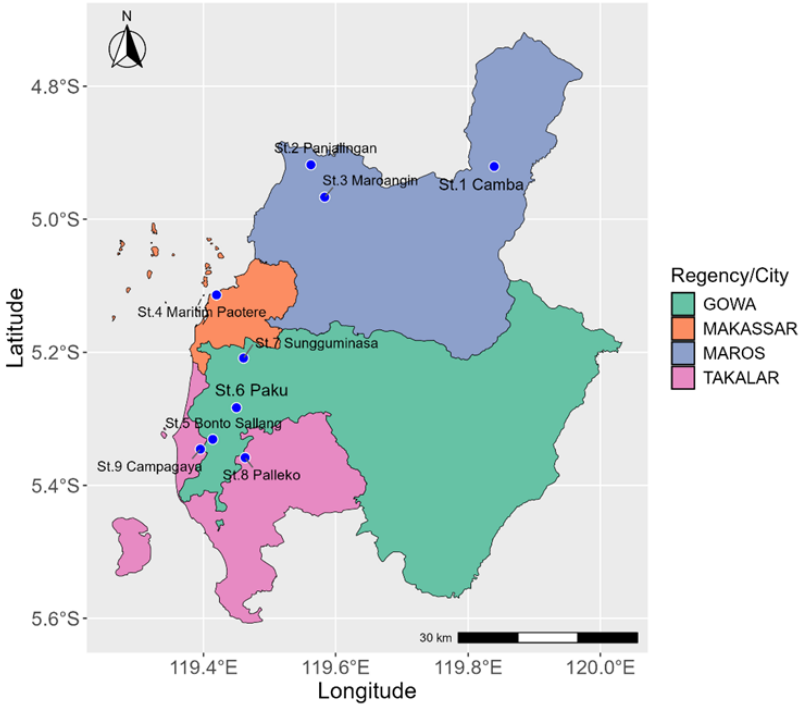

Figure 1. Location of study.

events. For accurate hydrological analysis based on the IDF curve, it is essential to estimate rainfall intensity. Such estimation based on short-term rainfall data can be carried out using an empirical approach, namely the Mononobe method [11]. The Mononobe method can also be applied to daily rainfall data when automatic rainfall records are not available in the observed area [12].

Before constructing the IDF curve, the first step is to determine the probability distribution of extreme rainfall, with the aim of estimating the design rainfall. Several probability distribution models commonly used by researchers include Pearson type III (PE3) distribution, log-normal (LN3) distribution, generalized extreme value (GEV) distribution, generalized Pareto (GPa) distribution, generalized logistic (GLo) distribution, and others [13]-[17]. Gnecco et al. [5] applied the GEV distribution to define the IDF curve in the Liguria region of Northern Italy. De Zoysa et al. [16] employed the Gumbel and PE3 distributions in developing the IDF curve in Sri Lanka. Noor et al. [6] utilized the Exponential, GPa, Gumbel, and GEV distributions to evaluate the IDF curve in Peninsular Malaysia. Ciupak et al. [13] applied the PE3, LN3, Weibull, log-gamma, and Gumbel distributions to develop the precipitation maximum time probability (PMAXTP) model in Poland.

Based on this description, this study adopts a probabilistic approach to determine the probability distribution that best fits the annual maximum daily rainfall data in the Mamminasata region, which comprises Makassar City, Maros Regency, Sungguminasa (the capital of Gowa Regency), and Takalar Regency. The selected distribution is then applied to estimate the design rainfall, and the resulting estimates are further used to construct the IDF curve.

2. MATERIALS AND METHODS

2.1. Probabilistic Models

Several probability distribution functions are frequently employed in the analysis of rainfall data [18], such as:

2.1.1. The GEV Distribution

The cumulative distribution function (CDF) of the GEV distribution is defined as Equation (1):

$$F(x) = \exp\left[-\exp\left(\kappa^{-1}log\left(1-\frac{\kappa}{\alpha}(x-\xi)\right)\right)\right], \quad (1)$$

where ξ denotes the location parameter, α the scale parameter, and κ the shape parameter. For $\kappa < 0$, $x \in \left(\xi+\frac{\alpha}{\kappa}, \infty\right)$, for $\kappa > 0$, $x \in \left(-\infty, \xi+\frac{\alpha}{\kappa}\right)$, and for $\kappa = 0$, the GEV distribution simplifies to the Gumbel distribution.

2.1.2. The GPa Distribution

The CDF of the GPa distribution is defined as Equation (2):

$$F(x) = 1-\exp\left(\kappa^{-1}log\left(1-\frac{\kappa}{\alpha}(x-\xi)\right)\right), \quad (2)$$

where ξ denotes the location parameter, α the scale parameter, and κ the shape parameter. For $\kappa < 0$, $x \in [\xi, \infty]$ for $\kappa > 0$, $x \in \left[\xi, \xi+\frac{\alpha}{\kappa}\right]$, for $\kappa = 0$, the GPa distribution is the Exponential distribution, and for $\kappa = 1$, the GPa distribution is the uniform distribution on $x \in [\xi, \xi + \alpha]$.

2.1.3. The GLo Distribution

The CDF of the GLo distribution is defined as Equation (3):

$$F(x) = \frac{1}{1+\exp\left(\kappa^{-1}log\left(1-\frac{\kappa}{\alpha}(x-\xi)\right)\right)}, \quad (3)$$

Table 2. the results of homogeneity tests.

Code	Pettitt Test			Buishand Range Test			SNHT Test		
	Break year	Statistics test	p_value	Break year	Statistics test	p_value	Break year	Statistics test
St. 1	2012	112	0.41	2012	1.31	0.17	2013	4.61
St. 2	2009	95	0.64	2009	1.26	0.22	1996	2.11
St. 3	2000	87	0.77	2000	1.16	0.34	2001	2.68
St. 4	2007	87	0.77	2007	1.32	0.16	2008	2.30
St. 5	2017	104	0.51	2017	1.12	0.39	2021	7.12
St. 6	2008	164	0.07	2008	1.24	0.25	2002	4.73
St. 7	1996	136	0.19	1996	1.89	**0.001**	1996	6.61
St. 8	2012	110	0.44	2014	1.15	0.36	2018	6.22
St. 9	2015	225	**0.003**	2016	2.11	**$5'10^{-5}$**	2018	**27.48**

The critical values of the SNHT test at 0.01 significance level are 10.198

PANDAWA INSTITUTE

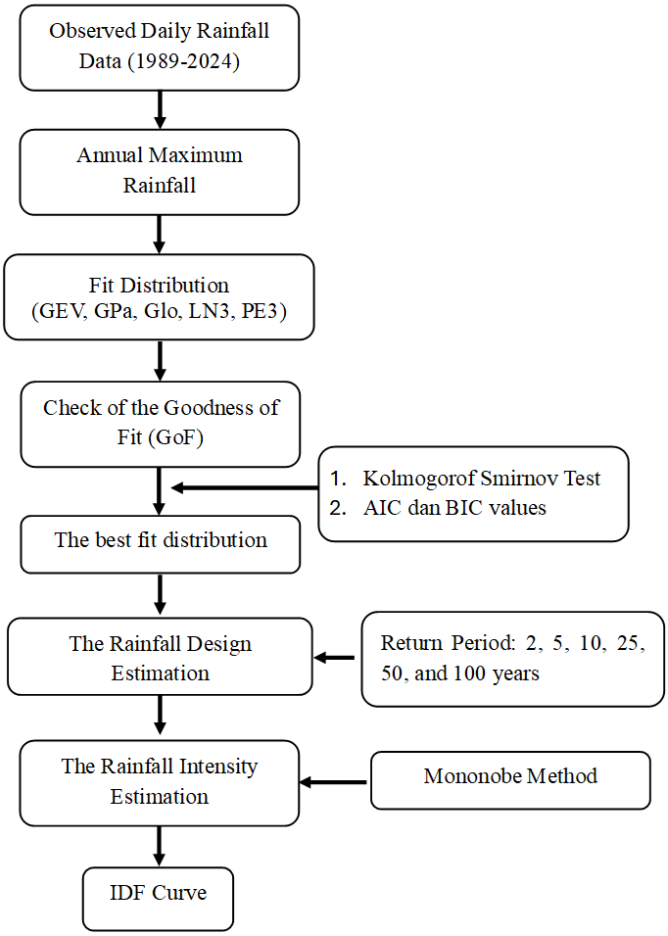

Figure 2. Flowchart illustrating the construction of the IDF curve.

where ξ denotes the location parameter, α the scale parameter, and κ the shape parameter. For $\kappa < 0$, $x \in \left(\xi + \frac{\alpha}{\kappa}, \infty\right)$, for $\kappa > 0$, $x \in \left(-\infty, \xi + \frac{\alpha}{\kappa}\right)$, and for $\kappa = 0$, the GLo distribution is the Logistic distribution.

2.1.4. The LN3 Distribution

The CDF of the LN3 distribution is defined as Equation (4):

$$F(x) = \Phi\left(-\kappa^{-1} log\left(1 - \frac{\kappa}{\alpha}(x - \xi)\right)\right) \quad (4)$$

where Φ (.) is a CDF of the standard normal distribution, ξ denotes the location parameter, α the scale parameter, and κ the shape parameter. For $\kappa < 0$, $x \in \left(\xi + \frac{\alpha}{\kappa}, \infty\right)$, for $\kappa > 0$, $x \in \left(-\infty, \xi + \frac{\alpha}{\kappa}\right)$, and for $\kappa = 0$, the LN3 distribution is the Normal distribution with parameters ξ and α.

2.1.5. The PE3 Distribution

The CDF of the PE3 distribution is defined as Equation (5):

$$F(x) = \frac{1}{\alpha\Gamma(\kappa)} \int_0^x \left(\frac{y - \xi}{\alpha}\right)^{\kappa - 1} exp\left(-\frac{y - \xi}{\alpha}\right) dy, \quad (5)$$

where ξ denotes the location parameter, α the scale parameter, κ the shape parameter, and Γ (.) is Gamma function.

2.1.6. The Rainfall Intensity Estimation

The distribution of rainfall as a function of time describes the variation in rainfall depth during a rainfall event. According to previous work, if automatic rainfall data are not available, rainfall intensity can be estimated using empirical methods [12], such as the Mononobe method, as shown in Equation (6):

$$I = \frac{R_{24}}{24}\left(\frac{24}{t}\right)^{\frac{2}{3}} \quad (6)$$

where I denotes the rainfall intensity for a rainfall duration of t (mm/h), t represents the rainfall duration (h), and R_{24} is the maximum 24-h rainfall (mm).

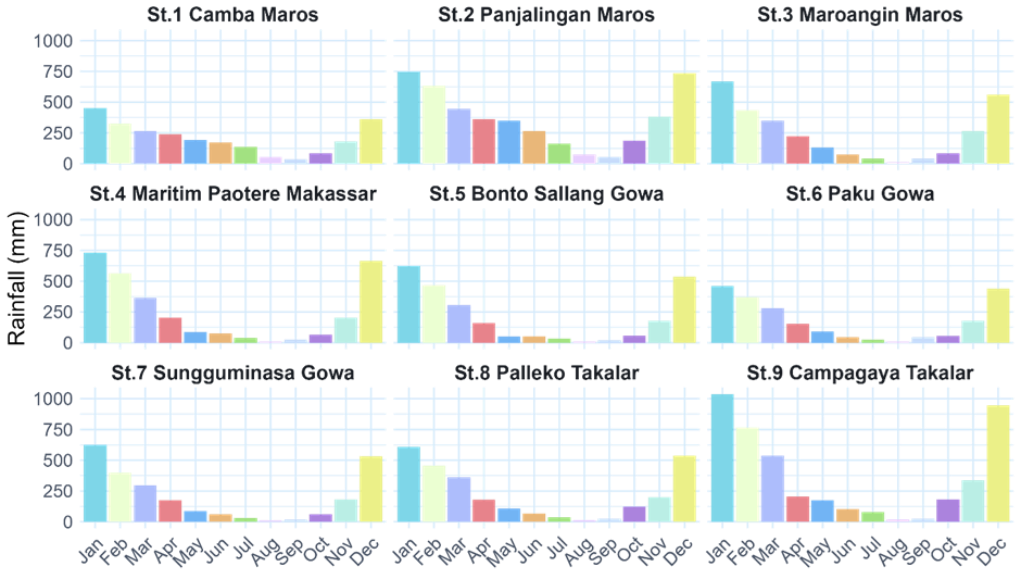

Figure 3. Distribution of the mean monthly rainfall.

Table 3. Statistical description of annual maximum daily rainfall data.

Code	n	Mean	Median	SD	Min	Max	Skewness	Kurtosis
St.1	36	113.36	98	41.62	57	207	0.64	-0.85
St.2	36	154.25	147	49.22	76	290	0.81	0.69
St.3	36	149.40	137	68.99	46	400	1.99	5.28
St.4	36	164.80	155.65	49.67	103	378	2.34	8.74
St.5	36	149.83	144.50	47.62	85	317	1.63	4.06
St.6	36	129.67	120	57.79	62	384	2.57	9.95
St.7	36	139.06	141.50	35.81	81	215	0.17	-0.71
St.8	36	141.94	118.50	104.89	61	710	4.79	25.99
St.9	36	207.64	145	167.37	78	790	2.002	3.79

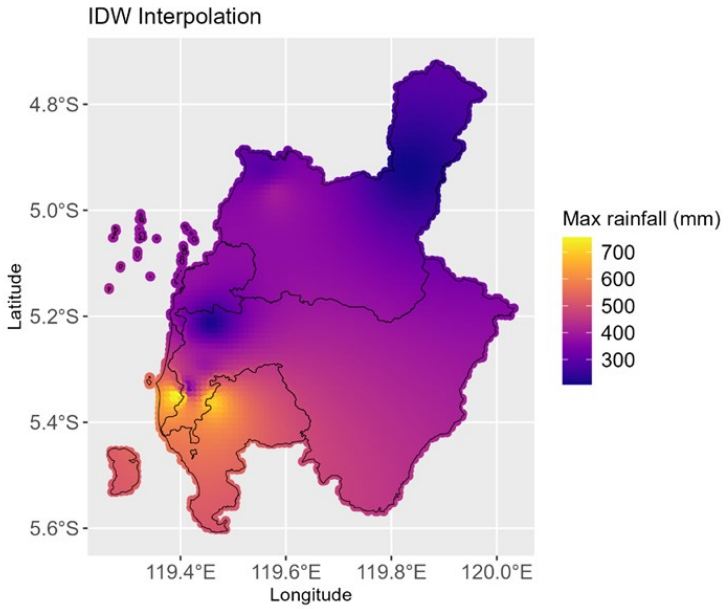

Figure 4. Spatial variability of maximum daily rainfall.

2.1.7. L-Moments

One of the methods that can be used in rainfall probability distribution modeling is the *L*-moment method. *L*-moments are sample statistical summaries that are analogous to conventional moments [18]. These *L*-moments provide information on measures of location, scale, skewness, kurtosis, and other characteristics related to the shape of the probability distribution of the sample data. *L*-moments are calculated linearly and provide more robust parameter estimates for data compared to other methods [19].

Let $x_{1:n} \leq \ldots \leq x_{n:n}$ denote the ordered sample, where n is the sample size. Hosking and Wallis [18] proposed an estimator for β_r as Equation (7):

$$b_r = \hat{\beta}_r = \frac{1}{n}\sum_{j=r+1}^{n}\frac{(j-1)(j-2)\ldots(j-r)}{(n-1)(n-2)\ldots(n-r)}x_{j:n}, \quad r = 1, 2, \ldots \quad (7)$$

The first four *L*-moments are given by Equations (8) – (11):

$$\lambda_1 = b_0 \quad (8)$$
$$\lambda_2 = 2b_1 - b_0 \quad (9)$$
$$\lambda_3 = 6b_2 - 6b_1 + b_0 \quad (10)$$
$$\lambda_4 = 20b_3 - 30b_2 + 12b_1 - b_0 \quad (11)$$

where λ_1 represents the measure of location (*L*-mean) and λ_2 represents the *L*-scale.

Hosking and Wallis [18] defined the *L*-moment ratios in extreme value analysis within the field of hydrology (Equations (12) – (14)) as follows:

$$\tau = \frac{\lambda_2}{\lambda_1}, 0 \leq \tau < 1 \quad (12)$$

$$\tau_3 = \frac{\lambda_3}{\lambda_2} \quad (13)$$

$$\tau_4 = \frac{\lambda_4}{\lambda_2} \quad (14)$$

where τ is the *L*-coefficient of variation (*L*-C_v), τ_3 is the *L*-skewness (*L*-C_s) and τ_4 is the *L*-kurtosis (*L*-C_k).

2.2. Data

This study utilized annual maximum daily rainfall data from 9 rainfall stations in Mamminasata region of South Sulawesi Province, covering the period from 1989 to December 2024. The rainfall stations were chosen based on the availability of complete data and extended observation period. The data was collected from the Water Resources, Human Settlements, Spatial Planning and Development Office of South Sulawesi province, and the Meteorology, Climatology and Geophysics Agency (https://dataonline.bmkg.go.id). The code, name, and location data of the rainfall stations are shown in Table 1, and location of all stations is displayed in Figure 1.

2.2.1. Homogeneity Tests

Accurate climate variability analysis requires prior homogeneity testing of rainfall datasets. A

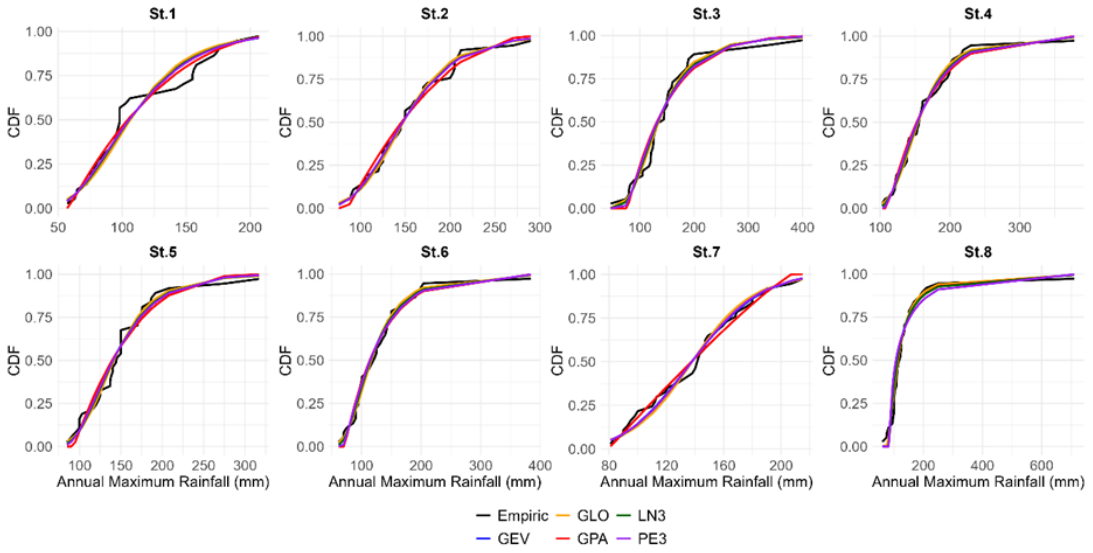

Figure 5. Plot of empirical data and five probability distributions.

Table 4. Goodness-of-Fit test for probability distributions.

Code/ Station	Distribution	K-S value (D)	Critical Value	The null hypothesis	AIC value	BIC value
	GEV	0.15	0.227	Accepted	75.52	80.27
	GPA	0.12	0.227	Accepted	112.41	117.17
St.1	GLO	0.16	0.227	Accepted	76.63	81.38
	LN3	0.15	0.227	Accepted	75.20	79.96
	PE3	0.14	0.227	Accepted	74.67*	79.41*
	GEV	0.08	0.227	Accepted	76.08*	80.83*
	GPA	0.09	0.23	Accepted	115.17	119.92
St.2	GLO	0.09	0.23	Accepted	76.31	81.06
	LN3	0.08	0.23	Accepted	76.03	80.78
	PE3	0.07	0.23	Accepted	76.06	80.81
	GEV	0.12	0.23	Accepted	82.30	87.05
	GPA	0.15	0.23	Accepted	154.11	158.86
St.3	GLO	0.10	0.23	Accepted	79.32*	84.07*
	LN3	0.13	0.23	Accepted	102.75	107.50
	PE3	0.14	0.23	Accepted	114.75	119.50
	GEV	0.05	0.23	Accepted	76.17*	80.92*
	GPA	0.09	0.23	Accepted	150.40	155.15
St.4	GLO	0.07	0.23	Accepted	75.80	80.55
	LN3	0.05	0.23	Accepted	76.81	81.56
	PE3	0.07	0.23	Accepted	115.25	120.00
	GEV	0.11	0.23	Accepted	77.14	81.89
	GPA	0.13	0.23	Accepted	155.44	160.19
St.5	GLO	0.10	0.23	Accepted	76.48*	81.23*
	LN3	0.11	0.23	Accepted	77.46	82.21
	PE3	0.12	0.23	Accepted	79.04	83.79
	GEV	0.06	0.23	Accepted	76.50	81.25
	GPA	0.10	0.23	Accepted	191.70	196.45
St.6	GLO	0.08	0.23	Accepted	75.84*	80.59*
	LN3	0.06	0.23	Accepted	78.03	82.78
	PE3	0.09	0.23	Accepted	118.07	122.82
	GEV	0.07	0.23	Accepted	76.04*	80.79*
	GPA	0.07	0.23	Accepted	77.21	81.96
St.7	GLO	0.08	0.23	Accepted	77.11	81.86
	LN3	0.07	0.23	Accepted	76.14	80.89
	PE3	0.07	0.23	Accepted	76.12	80.87
	GEV	0.12	0.23	Accepted	138.7	143.45
	GPA	0.16	0.23	Accepted	226.99	231.74
St.8	GLO	0.12	0.23	Accepted	115.91*	120.66*
	LN3	0.16	0.23	Accepted	190.52	195.27
	PE3	0.23	0.23	Rejected	223.08	227.83

* The best distribution

PANDAWA INSTITUTE

Table 5. Parameter estimation using Bootstrap method for the best distribution.

Code/ Station	Distribution	Parameter estimation (mean and 95% CI)		
		Location	Scale	Shape
St.1	PE3	113.28	42.01	1.11
		(99.55, 127.17)	(33.14, 49.63)	(0.05, 1.99)
St.2	GEV	133.76	40.62	0.06
		(119.43, 150.03)	(30.36, 51.73)	(-0.15, 0.31)
St.3	GLo	135.85	28.74	-0.25
		(120.76, 150.57)	(19.25, 39.87)	(-0.41, 0.03)
St.4	GEV	143.69	30.74	-0.08
		(132.79, 156.41)	(21.25, 39.85)	(-0.36, 0.27)
St.5	GLo	142.23	22.08	-0.19
		(128.07, 155.29)	(15.82, 29.61)	(-0.35, 0.06)
St.6	GLo	117.81	23.16	-0.26
		(103.19, 133.43)	(16.36, 31.78)	(-0.46, -0.53)
St.7	GEV	126.05	34.33	0.24
		(112.17, 140.00)	(27.26, 40.96)	(0.01, 0.48)
St.8	GLo	117.02	21.96	-0.44
		(105.48, 129.68)	(13.96, 33.85)	(-0.66, -0.09)

homogeneous climatic series is characterized by variability attributable only to natural weather and climate processes. Therefore, inhomogeneous series should be detected and either adjusted or removed before further analysis. In this study, three tests were used to detect inhomogeneity in the data series: the Pettitt test, the Buishand Range Test, and the Standard Normal Homogeneity Test (SNHT). According to Suhaila [20], the performance of the three homogeneity tests is assessed by classifying the results into three categories. A series is labeled class A (useful) when none or only one test rejects the null hypothesis at the 1% significance level, indicating no evident inhomogeneity. Class B (doubtful) includes series for which two tests reject the null hypothesis, suggesting possible inhomogeneities and requiring cautious interpretation. Class C (suspect) refers to series in which all three tests reject the null hypothesis; such series should be excluded from trend and variability analyses.

Table 2 presents the results of the homogeneity tests for each rainfall station. The Pettitt and SNHT tests indicate that only station 9 is significant at the 1% significance level. Meanwhile, the Buishand Range test shows significant results at the 1% level for stations 7 and 9. Based on the homogeneity classification proposed [20], it is concluded that the data series at station 9 is inhomogeneous and therefore excluded from further analysis.

2.3. Construction of IDF curves

Figure 2 shows a flowchart for constructing the IDF curve. The annual maximum rainfall data were fitted to five probability distributions. The best-fitting distribution was selected based on the Kolmogorov–Smirnov (K–S) test [13]. If more than one distribution satisfied the K–S test, the final selection was made based on the smallest AIC and BIC values [13]. The uncertainty of the probability distribution parameters and their confidence intervals was estimated using the bootstrap method through resampling [21]. The initial values of the distribution parameters applied in the bootstrap procedure were obtained using the L-moment method [22]. The next step involves estimating return levels using the parameters of the best-fitting probability distribution for return periods of 2, 5, 10, 25, 50, and 100 years. The corresponding confidence intervals for the return levels are then

Table 6. Estimated return levels of rainfall with 95% confidence intervals.

Code/ Station	Return levels (95% CI)					
	2-year	5-year	10-year	25-year	50-year	100-year
St.1	150.83	155.93	158.78	161.94	164.06	166.02
	(130.92, 170.73)	(125.02, 186.84)	(121.95, 195.61)	(120.53, 203.35)	(120.83, 207.29)	(121.78, 210.26)
St.2	148.81	197.51	231.63	276.99	312.35	348.95
	(130.97, 166.66)	(162.93, 232.10)	(177.79, 285.47)	(188.47, 365.50)	(189.92, 434.78)	(185.33, 512.57)
St.3	157.60	192.80	225.32	277.95	326.59	384.43
	(138.37, 176.83)	(159.69, 225.90)	(172.82, 277.82)	(184.08, 371.81)	(185.74, 467.47)	(178.77, 590.08)
St.4	154.79	187.14	207.00	230.44	246.72	262.00
	(140.62, 168.97)	(158.66, 215.62)	(163.72, 250.28)	(162.92, 297.96)	(157.70, 335.74)	(149.08, 374.92)
St.5	158.59	183.80	206.01	240.24	270.39	304.79
	(142.38, 174.79)	(159.38, 208.22)	(169.89, 242.13)	(179.45, 301.03)	(182.47, 358.31)	(180.81, 428.77)
St.6	135.40	164.10	190.83	234.43	275.05	323.69
	(116.29, 154.51)	(135.08, 193.11)	(147.51, 234.14)	(158.61, 310.26)	(160.79, 389.31)	(155.21, 492.18)
St.7	139.20	188.03	228.49	291.22	347.90	414.47
	(123.35, 155.05)	(156.90, 219.16)	(175.91, 281.07)	(193.17, 389.26)	(198.21, 497.59)	(193.48, 635.45)
St.8	134.82	168.44	204.57	272.83	346.19	445.71
	(117.21, 152.43)	(130.95, 205.93)	(134.96, 271.19)	(122.41, 423.25)	(88.48, 603.90)	(18.38, 873.04)

determined using a resampling method. Using the design rainfall (return level) estimates for return periods of 2, 5, 10, 25, 50, and 100 years, rainfall intensity was calculated with the Mononobe method. Finally, the IDF curve was developed from the estimated intensities for durations of 1, 2, 3, 6, 12, and 24 h, corresponding to return periods of 2, 5, 10, 25, 50, and 100 years.

3. RESULTS AND DISCUSSIONS

3.1. Description of Rainfall Data

Based on Figure 3, it can be observed that in all locations, peak rainfall occurs in December and January, indicating that these months are characterized by heavy rainfall throughout the region. In contrast, the dry season typically occurs in August and September. For further analysis, the annual maximum daily rainfall data were used. A description of these data is presented in Table 3 and Figure 4. Table 3 shows that the mean annual maximum daily rainfall over the 36-year period in the Mamminasata region ranges from 113 to 208 mm. The minimum value, 46 mm, was recorded at station 3 (Maroangin, Maros), while the maximum value, 790 mm, occurred at station 9 (Campagaya, Takalar). The skewness values are all positive, indicating that the data distributions are skewed to the right and generally exhibit a sharp peak. Figure 4 shows that the northern part of the Mamminasata region experiences lower daily maximum rainfall, whereas the southwestern part exhibits higher daily maximum rainfall.

3.2. Fitting Probability Density Functions and Estimation of Their Parameters

Figure 5 illustrates the comparison between empirical data and five fitted probability distributions. Visually, all distributions exhibit a close alignment with the empirical curve across most quantiles. These visual assessments are supported by the results of the Kolmogorov–Smirnov test, as well as the Akaike Information Criterion (AIC) and Bayesian Information Criterion (BIC) presented in Table 4, which collectively aid in identifying the best-fitting model for annual maximum daily rainfall data. As shown in Table 4, all stations fit the five candidate distributions, with

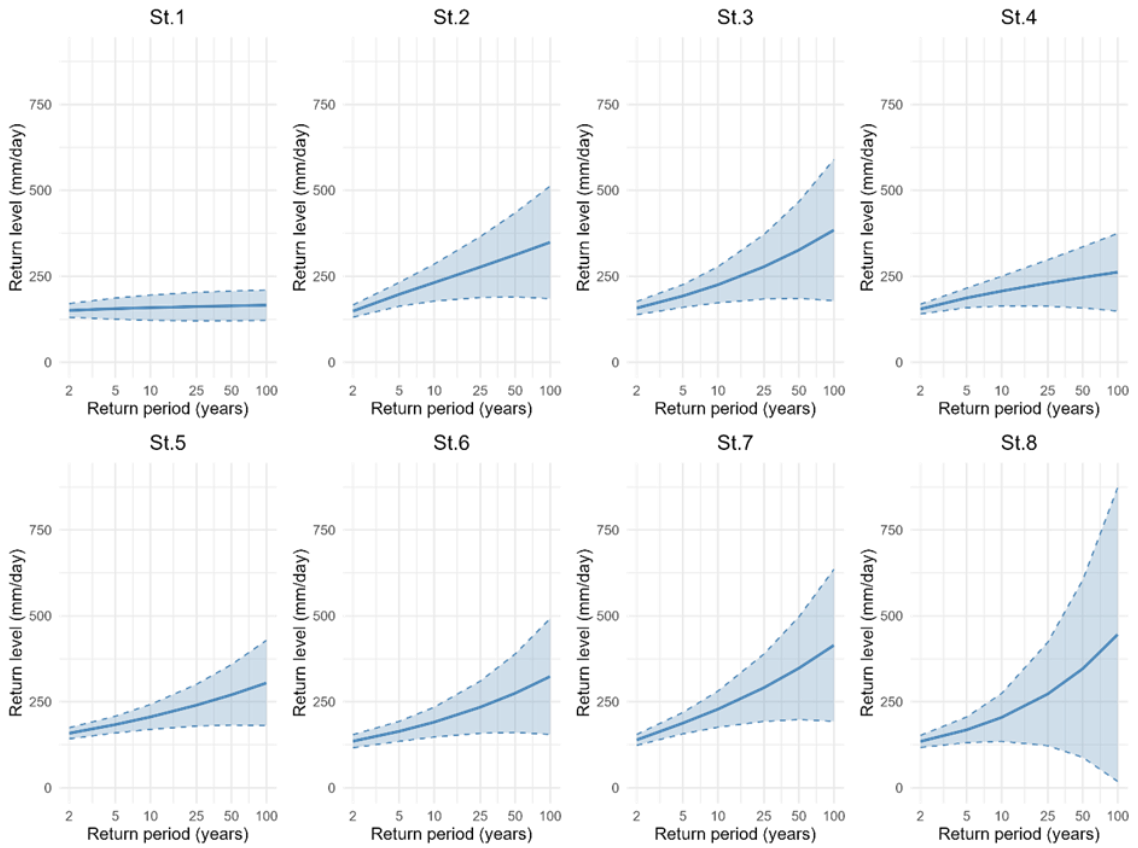

Figure 6. Return level plots of annual maximum daily rainfall.

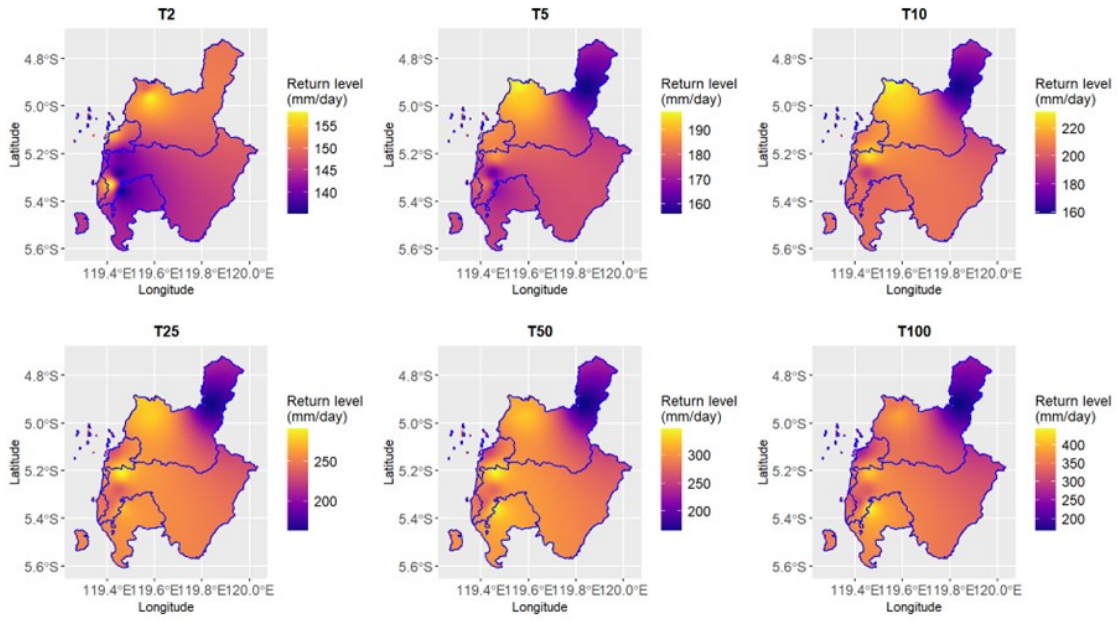

Figure 7. Spatial distribution of the return levels (T2–T100) in the Mamminasata region.

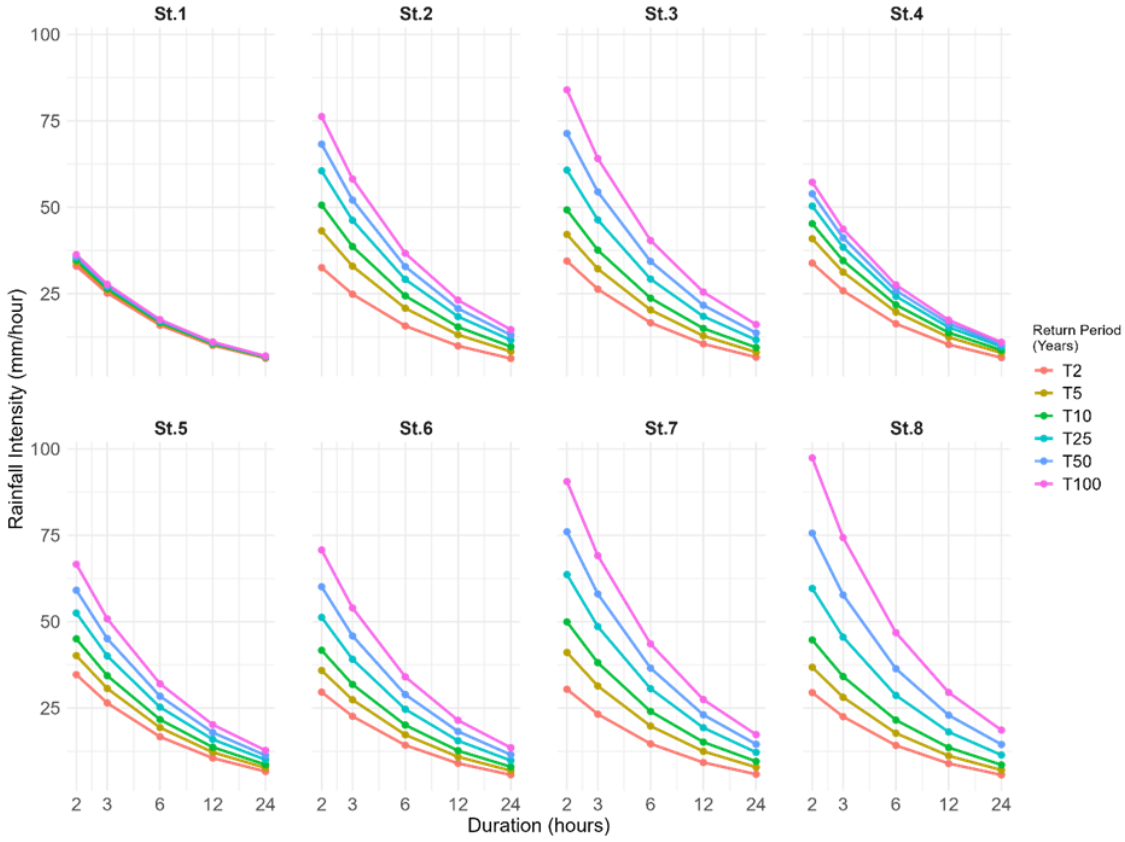

Figure 8. The IDF curve for each station.

PANDAWA INSTITUTE

Table 7. The discordancy measure (D) for each station.

Code/ Station	D	Station	D	Critical value (N=8)
St.1	1.83	St. 5	0.54	2.14
St.2	0.21	St. 6	0.20	
St.3	1.05	St. 7	1.00	
St.4	1.63	St. 8	1.53	

Table 8. The regional fitting distribution.

Distribution	L-Skewness	p-value	RMSE	Parameter estimation		
				Location	Scale	Shape
GEV	1.019	0.998	23.9	118.13	35.33	-0.11
GLO	0.78	0.9797	18.97	132.20	24.83	-0.24

Table 9. Estimated return levels of rainfall for the GEV and GLO distributions.

Distribution	Return levels (95% CI)					
	2-year	5-year	10-year	25-year	50-year	100-year
GEV	131.35	175.73	208.30	253.46	290.13	329.43
GLO	132.20	173.10	204.20	250.96	292.68	341.47
Absolute difference	0.86	2.64	4.10	2.50	2.55	12.05

the exception of station 8, where the data does not fit the PE3 distribution. The selection of the best-fitting distribution for each station is based on the lowest AIC and BIC values. Accordingly, the best distributions are as follows: PE3 for Station 1, GLo for stations 3, 5, 6, and 8, GEV for stations 2, 4 and 7.The estimated parameters for each selected distribution are provided in Table 5.

The results of this study are consistent with the findings of Sanusi et al. [23], which indicate that the annual maximum rainfall data in Gowa Regency follow the PE3, LN3, and GLo distributions.

3.3. The Return Levels and IDF Curves

The estimated parameters of the best-fit distributions in Table 5 were subsequently used to calculate the return level for each station, corresponding to return periods of 2, 5, 10, 25, 50, and 100 years (Table 6). The results present the estimated return levels of maximum rainfall for return periods ranging from 2 to 100 years at the eight rainfall stations, together with their associated uncertainty bounds. For all stations, return levels increase monotonically with increasing return period, indicating a higher magnitude of extreme rainfall events at longer recurrence intervals (Figure 6). Station 1 consistently shows the lowest return levels, indicating relatively milder extreme rainfall conditions. Stations 1 and 4 exhibit relatively stable return levels with narrow confidence intervals indicating consistent rainfall patterns. The estimated return levels for the 2-year and 5-year return periods at station 4 are 154.79 and 187.14 mm/day, respectively. These values are not significantly different from the previous findings [24], who reported estimated return levels of 144.675 and 188.624 mm/day for the same return periods. In contrast, stations 7 and 8 exhibit the highest return levels, particularly for long return periods, suggesting a greater exposure to extreme rainfall events. These differences highlight the heterogeneous nature of extreme rainfall characteristics in the Mamminasata region, which may be attributed to local climatic influences, topography, and proximity to moisture sources. The uncertainty associated with return level estimates increases substantially with increasing return period, as indicated by the widening confidence intervals. This pattern is especially pronounced for return periods exceeding 50 years and is most evident at stations 7 and 8. For shorter return periods (2–10 years), the confidence intervals are

relatively narrow across all stations.

The spatial distribution of rainfall the return levels for different return periods (T2–T100) illustrates the interpolated spatial variability of extreme rainfall across the Mamminasata region based on station-derived estimates (Figure 7). Rainfall the return levels increase consistently with increasing return period at all locations, indicating a progressive intensification of extreme rainfall events for rarer occurrences. Spatially, higher return levels are predominantly observed in the western and northwestern parts of the study area, whereas relatively lower values are found in the southern and southeastern regions. The persistence of this spatial pattern across all return periods suggests that the spatial variability of extreme rainfall is systematic and likely influenced by regional climatic and topographic controls rather than random local extremes

These design rainfall values were then applied to determine the estimation of rainfall intensity for durations of 2, 3, 6, 12, and 24 h. The resulting IDF curves are presented in Figure 8. In the IDF curve, the x-axis represents the rainfall duration (in hours), while the y-axis indicates the estimated rainfall intensity (in mm/hour). These curves are presented for various return periods. As shown in Figure 8, for all stations, rainfall intensity decreases systematically with increasing duration, while higher return periods consistently correspond to higher rainfall intensities. This behavior confirms the expected theoretical characteristics of IDF relationships and indicates that the fitted probability distributions adequately capture the extreme rainfall behavior. At shorter durations (2–3 hours), the highest rainfall intensities are observed, particularly for long return periods. Stations 7 and 8 exhibit the largest intensities, reaching approximately 90–100 mm/h for the 100-year return period at a 2-h duration, whereas station 1 shows the lowest intensities across all return periods and durations. These spatial differences highlight the pronounced variability of extreme rainfall across the study area, likely influenced by local climatic and topographic conditions.

As rainfall duration increases, the differences in intensity between return periods gradually diminish, especially for durations longer than 12 h. At 24-h duration, rainfall intensities across all stations converge to relatively lower values, reflecting the transition from short-duration convective rainfall to longer-duration rainfall processes. This convergence further supports the physical consistency of the estimated IDF curves. Based on Figure 1, the eight rainfall stations in the Mamminasata region are geographically close, therefore, Regional Frequency Analysis (RFA) was applied in this study. The annual maximum rainfall

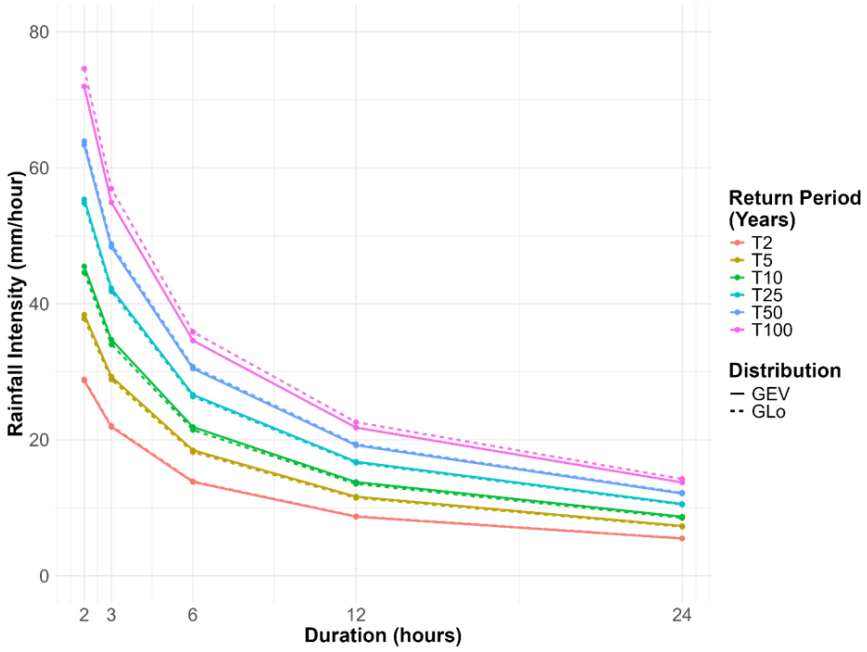

Figure 9. The IDF curve for Mamminasata region.

data from the eight stations were found to be statistically homogeneous, as indicated by the heterogeneity measures ($H_1 = 0.86 < 1$ and $H_2 = 0.85 < 1$) according to the criteria of Hosking and Wallis. In addition, Table 7 shows that all stations have discordancy measures (D) lower than the corresponding critical values, indicating that none of the stations is discordant.

The distribution functions used to estimate rainfall magnitudes in the Mamminasata region are the Generalized Extreme Value (GEV) and the Generalized Logistic (GLO) distributions. The goodness-of-fit results presented in Table 8 indicate that both the GEV and GLO distributions are suitable for estimating rainfall return levels in the Mamminasata region. The estimated return levels for both distributions are summarized in Table 9, which shows that the return level estimates from the two distributions do not differ significantly. Furthermore, the IDF curves for the Mamminasata region are presented in Figure 9.

Figure 9 illustrates the relationship between rainfall intensity and duration for different return periods. The results show a consistent decrease in rainfall intensity with increasing duration across all return periods. Higher return periods are associated with greater rainfall intensities, particularly for short durations, reflecting more extreme rainfall events. The separation between the IDF curves is more pronounced at short durations and gradually diminishes at longer durations, indicating that rainfall variability is more dominant at shorter timescales. The smaller spacing between the curves at longer durations suggests more homogeneous regional rainfall characteristics. Overall, the regional IDF curves provide stable estimates and can be reliably used for hydrological design in the Mamminasata region.

4. CONCLUSIONS

This study focused on identifying probability distributions that best represent the annual maximum daily rainfall data in the Maminasata region, which comprises nine locations. The results indicate that the distribution models vary across stations, suggesting that each location exhibits distinct statistical characteristics. This highlights the importance of considering the probability distribution types for data when constructing IDF curves. These findings underscore the need to employ multiple distribution models to accurately capture the variability and extremes of rainfall patterns across different locations. The results also show a general that the longer the rainfall duration, the lower the intensity. Likewise, shorter return periods are associated with lower intensities. However, at certain stations, rainfall intensities remain nearly constant across all return periods for each given duration. This study has limitations, as it does not explicitly address the treatment of non-stationarity in the data. Future research will focus on non-stationary modeling of extreme rainfall with time-varying parameters to capture climate variability and change, and on applying multivariate GEV models for a more comprehensive understanding of regional rainfall extremes.

AUTHOR INFORMATION

Corresponding Author

Wahidah Sanusi — Department of Mathematics, Universitas Negeri Makassar (UNM), Makassar-90224 (Indonesia);
orcid.org/0000-0002-1530-7553
Email: wahidah.sanusi@unm.ac.id

Authors

Sudarmin Patahuddin — Department of Statistics, Universitas Negeri Makassar (UNM), Makassar-90224 (Indonesia);
orcid.org/0009-0007-4902-6200

Sahlan Sidjara — Department of Mathematics, Universitas Negeri Makassar (UNM), Makassar-90224 (Indonesia);
orcid.org/0000-0003-4273-2499

Author Contributions

W. S. was responsible for the conceptualization of the study, the development of the methodology, the execution of the formal analysis, and the processing of rainfall data. S. P. contributed to the data analysis, prepared the data visualization, and provided critical input through review and editing of the manuscript. S. S. was in charge of data collection and assisted in preparing the original draft of the manuscript. All authors read and approved the final version of the manuscript.

Conflicts of Interest

The authors declare no conflict of interest.

ACKNOWLEDGEMENT

The authors would like to thank the Ministry of Higher Education, Science, and Technology of Indonesia for their financial support, specifically through grant number 2973/UN36.11/TU/2025. The authors also extend their gratitude to the staff of the Water Resources, Human Settlements, Spatial Planning, and Development Office of South Sulawesi Province for providing the rainfall data.

DECLARATION OF GENERATIVE AI

Not applicable.

REFERENCES

[1] D. Kusumaningrum, T. A. Hafsari, D. Rachmawan, D. Hidayati, R. Siburian, Sudiyono, R. Cahyadi, and R. Indrawasih. (2026). In: "Managing Disruption and Developing Resilience for a Better Southeast Asia, (Springer Proceedings in Humanities and Social Sciences, ch. Chapter 49". 701-716. 10.1007/978-981-96-2116-3_49.

[2] Mulyadi and M. Nursyahputra. (2020). "Planning ecotourism based on GIS in Gowa South Sulawesi". *IOP Conference Series: Earth and Environmental Science.* **575** (1). 10.1088/1755-1315/575/1/012055.

[3] S. Wulandari, F. Pratama, N. Andika, P. Wongso, W. Wijayasari, and F. I. W. Rohmat. (2025). "Identifying dominant river contributions to urban flooding: a scenario-based study of Makassar City". *Frontiers in Built Environment.* **11**. 10.3389/fbuil.2025.1612416.

[4] A. Ulfiana, M. Arsyad, and P. Palloan. (2023). "The Atmospheric Dynamics Related to Extreme Rainfall and Flood Events during September-October-November in South Sulawesi". *Forum Geografi.* **37** (2). 10.23917/forgeo.v37i2.22339.

[5] I. Gnecco, A. Palla, P. La Barbera, G. Roth, and F. Giannoni. (2023). "Defining Intensity Duration-Frequency Curves at Short Durations: A Methodological Framework". *Hydrological Sciences Journal.* **68** (11): 1499 -1512. 10.1080/02626667.2023.2224002.

[6] M. Noor, T. Ismail, S. Shahid, Asaduzzaman, and A. Dewan. (2021). "Evaluating Intensity-Duration-Frequency (IDF) Curves of Satellite -Based Precipitation Datasets in Peninsular Malaysia". *Atmospheric Research.* **248** : 105203. 10.1016/j.atmosres.2020.105203.

[7] T. S. Alsumaiti, K. A. Hussein, D. T. Ghebreyesus, P. Petchprayoon, H. O. Sharif, and W. Abdalati. (2024). "Development of Intensity-Duration-Frequency (IDF) Curves over the United Arab Emirates (UAE) Using CHIRPS Satellite-Based Precipitation Products". *Remote Sensing.* **16** : 27. 10.3390/rs16010027.

[8] A. Al Mamoon, N. E. Joergensen, A. Rahman, and H. Qasem. (2014). "Derivation of New Design Rainfall in Qatar Using L-Moment Based Index Frequency Approach". *International Journal of Sustainable Built Environment.* **3** : 111-118. 10.1016/j.ijsbe.2014.07.001.

[9] I. H. Elsebaie. (2012). "Developing Rainfall Intensity-Duration-Frequency Curves Relationship for Two Regions in Saudi Arabia". *Journal of King Saud University: Engineering Sciences.* **24** : 131-140. 10.1016/j.jksues.2011.06.001.

[10] F. F. De Paola, M. Giugni, M. E. Topa, and E. Bucchignani. (2012). "Intensity-Duration-Frequency (IDF) Rainfall Curves for Data Series and Climate Projection in African Cities". *SpringerPlus.* **3** (133): 1-18. 10.1186/2193-1801-3-133.

[11] F. Faradiba. "Analysis of Intensity, Duration, and Frequency Rain Daily of Java Island Using Mononobe Method". **1783** : 012107. 10.1088/1742-6596/1783/1/012107

[12] A. W. Susilowati, A. A. Alisjahbana, and D. I. Kusumastuti. (2022). "Estimation of Intensity Duration Frequency for Ungauged Basin in Lampung Province, Indonesia". *International Journal of Design and Nature and Ecodynamics.* **17** (2): 297-302. 10.18280/ijdne.170217.

[13] M. Ciupak, B. Ozga-Zielinski, T. Tokarczyk, and J. Adamowski. (2021). "A Probabilistic

PANDAWA INSTITUTE

Model for Maximum Rainfall Frequency Analysis". *Water.* **13** : 2688. 10.3390/w13192688.

[14] G. J. Grundemann, E. Zorzetto, H. E. Beck, M. Schleiss, N. van de Giesen, M. Marani, and R. J. van der Ent. (2023). "Extreme Precipitation Return Levels for Multiple Durations on a Global Scale". *Journal of Hydrology.* **621** : 129558. 10.1016/j.jhydrol.2023.129558.

[15] A. Mursadin and E. Zeannyta. (2021). "Metode Praktis Estimasi Model-Model Probabilistik pada Analisis Frekuensi Banjir untuk Praktisi Penyelenggara Infrastruktur di Kalimantan Selatan". *Jurnal Kacapuri: Jurnal Keilmuan Teknik Sipil.* **4** (1). 10.31602/jk.v4i1.5155.

[16] S. De Zoysa, J. Sirisena, H. Perera, S. Fernando, M. Gunathilake, and U. Rathnayake. (2024). "Development of Intensity-Duration-Frequency Curves for Sri Lanka Using Satellite-Based Precipitation Products: Understanding Environmental Conditions and Concerns". *Case Studies in Chemical and Environmental Engineering.* **9** : 100713. 10.1016/j.cscee.2024.100713.

[17] H. Aksu, H. Aksoy, M. Cetin, S. G. Yaldiz, I. Yildirim, and O. Alsenjar. (2025). "Development of Rainfall Intensity-Duration-Frequency Curves under Nonstationary Conditions". *Sustainable Water Resources Management.* **1** : 4. 10.1007/s40899-024-01176-2.

[18] J. R. M. Hosking and J. R. Wallis. (1997). "Regional Frequency Analysis: An Approach Based on L-Moments". Cambridge University Press, London. 10.1017/CBO9780511529443.

[19] S. S. Eslamian and H. Feizi. (2007). "Maximum Monthly Rainfall Analysis Using L-Moments for an Arid Region in Isfahan Province, Iran". *Journal of Applied Meteorology and Climatology.* **46** : 494-503. 10.1175/JAM2465.1.

[20] J. Suhaila, S. M. Deni, and A. A. Jemain. (2008). "Detecting Inhomogeneity of Rainfall Series in Peninsular Malaysia". *Asia-Pacific Journal of Atmospheric Sciences.* **44** : 369-380.

[21] Z. Jiao, M. A. Alam, J. Yuan, C. Farnham, and K. Emura. (2024). "Prediction of Extreme Rainfall Events in the 21st Century: The Results Based on Bayesian Markov Chain Monte Carlo". *Urban Climate.* **53** : 101822. 10.1016/j.uclim.2024.101822.

[22] Z. Khan, A. Rahman, and F. Karim. (2023). "An Assessment of Uncertainties in Flood Frequency Estimation Using Bootstrapping and Monte Carlo Simulation". *Hydrology.* **10** (18): 1-16. 10.3390/hydrology10010018.

[23] W. Sanusi, S. Chaerunnisa, S. Annas, S. Side, and M. Abdy. (2022). "Estimated Parameters of Rain Flow Distribution Using L-Moment Method in South Sulawesi, Indonesia". *Journal of Applied Mathematics and Computation.* **6** (1): 30-40. 10.26855/jamc.2022.03.006.

[24] N. Sunusi, Giarno, Muflihah, and N. A. Muzakir. (2024). "Return Levels on Stationary Extreme Rainfall Series: A Comparative Study of Generalized Extreme Value and Generalized Pareto Distributions". *Environment and Ecology Research.* **12** (2): 109-120. 10.13189/eer.2024.120202.